Supporting Information

Acid-inducing {110}/{121} Facet Junction Formation Boosting the Selectivity and Activity on CO_2 Photoreduction of $BaTiO_3$ Nanoparticles

Weihua Cai, [#a] Yabo Wang, [#a] Lei Zhao, [b] Xun Sun, [c] Jun Xu, [c] Jin Chen, [a] Ruochen Shi, [a] Peihong Ma, [a] Meidan Que [*a]

[a] *Shaanxi Key Laboratory of Nano Materials and Technology, College of Materials Science and Engineering, Xi'an University of Architecture and Technology, Xi'an 710055, P. R. China. Email: mdque@xauat.edu.cn*
[b] *School of Physics and Opto-Electronic Technology, Baoji University of Arts and Sciences, Baoji, Shanxi 721016, P. R. China*
[c] *Institute of Guizhou Aerospace Measuring and Testing Technology, Guiyang 550009, P. R. China*
[#] *Both authors have an equally contribution.*

Experimental

Materials

Hydrofluoric acid (Aladdin, AR, ≥ 40.0 %, HF), tetrabutyl titanate (Aladdin, ≥ 99.0 %), sodium hydroxide (Zhiyuan Chemical Reagent Co., LTD, 96.0 %, NaOH), hydrochloric acid (Sinopharm, 36.0 ~ 38.0 %, HCl), barium hydroxide octahydrate (Sinopharm, 98.0 %, $Ba(OH)_2 \cdot 8H_2O$), glyoxal (Aladdin, 40 *wt.* % in H_2O, $C_2H_2O_2$).

Synthesis of wheat-heading $BaTiO_3$

25 mL 1 M acetic acid solution was prepared, and 0.7579 g barium nitrate weighed by an analytical balance was added into the acetic acid solution, which was solution A. Solution B was obtained by taking 10 mL of anhydrous ethanol and adding 0.1665 g of titanium dioxide into it. Mix solution A and B and stir for 10 min. Add 1.0000 g sodium hydroxide into the mixed solution, add magnetons into the teflon lining, stirring for 1 h, put the teflon lining into the reaction kettle, react at 200℃ for 24 h, and cool with the furnace. After cooling the reactor, soak the precipitate in 0.1 M hydrochloric acid solution, citric acid solution, acetic acid solution and the mixed solution of hydrochloric acid: citric acid (3:7, 5:5, 7:3) for 1 h, centrifuge at 9000 rpm for 5 min to centrifuge the precipitate, clean the precipitate with deionized water to neutral, and put it in the oven for drying. Finally, the dried powder was placed in Muffle furnace at 900℃ for 2 h to obtain $BaTiO_3$ nanoparticles.

Characterization

The structure and crystallinity of the samples were recorded by using X-ray diffraction (XRD) analysis on the Rigaku Smartlab diffractometer with Cu-Kα radiation at a scanning rate of 10° min^{-1}. Transmission electron microscopy (TEM), high-resolution transmission electron microscopy (HR-TEM) and energy dispersive X-ray spectroscopy (EDX) were obtained using Talos F200X. X-ray photoelectron spectroscopy (XPS) measurements were performed on Thermo Scientific K-Alpha to characterizing the chemical states and surface composition of samples, and the data were calibrated according to the peak of C 1s (284.6 eV). The static water contact-angle was measured by JC2000DM. Brunauer-Emmett-Teller (BET) of samples were measured using Micromeritics ASAP 2020 surface area and porosity analyzer. UV-vis diffuse reflectance spectra (DRS) were tested using a UV-vis spectrophotometer (Cary 5000, USA). Photoluminescence (PL) spectra was measured by PTI Quanta Master 40, USA. The Time-resolved PL (TRPL) was collected by a FLS980 with the laser of 350

nm.

Photocatalytic CO_2 reduction

The CO_2 conversion reaction was carried out in a 100 mL sealed stainless-steel reactor. 50 mg catalyst and 2 mL deionized water were placed in a container in the reactor. After the reaction kettle is closed, CO_2 gas was injected for 10 min. After the air inside the cavity is cleared, the gas valve is closed to ensure that 0.2 Mpa pressure in the reaction kettle. The CO_2 reduction reaction was then performed under light, and the time was recorded. 300 W Xe lamp with model CEL-HXF300-(T3) (Beijing Zhongjiao Jinyuan Technology Co., LTD) was used as the analog fluorescent lamp. The collected gas was injected into gas phase spectrometer with model GC-7920 (Beijing Zhongjiao Jinyuan Technology Co., LTD) for testing, and the final test results were obtained.

Photoelectrochemical tests

The electrochemical workstation CHI660E B20068C was used for the photoelectric chemistry test. A standard three-electrode system was used, with drops of the sample on indium-tin-oxide (ITO) glass as the working electrode, Ag/AgCl as the reference electrode and Pt as the counter electrode. 0.1 mol/L^{-1} of Na_2SO_4 solution was used as the electrolyte and the light source was a 300 W Xe lamp providing simulated solar irradiation.

Electrochemical Impedance Spectroscopy (EIS). The EIS was tested by the electrochemical workstation with "A.C Impedance" options under light, light and ultrasonic conditions. Then, the equivalent circuit diagram was simulated using Zview software.

Linear Sweep Voltammetry (LSV). The LSV was characterized by the electrochemical workstation with "Linear Sweep Voltammetry" options under light, light and ultrasonic conditions.

Mott-Schottky. The Mott-Schottky was obtained by the electrochemical workstation with "Impedance-Potential" at different frequencies (500, 1000, 1500 Hz).

Cyclic voltammetry. The cyclic voltammetry (C-V) of the catalysts were recorded using an electrochemical workstation with "Cyclic Voltammetry" and -0.5 to 0.5 V is used as the voltage range.

DFT theoretical calculation

In this work, the Gibbs free energy of $BaTiO_3$ was calculated using Materials Studio 2017. Generalized Gradient Approximation and Perdew Burke Ernzerhof exchange functional were used to calculate the correlation performance. In order to achieve

accurate density of electronic states, the plane wave cutoff energy was set to 400 eV, and 3×3×3 is adopted for all K-point grids. The maximum force tolerance of 0.05 eV/ A was used to obtain good convergence results. Cut the surface along the projected $BaTiO_3$ [001], using A 10 A vacuum thickness in the z direction to avoid the interaction between periodic mirror images. The structure of all models was optimized, the bottom two layers were fixed, and the top atom was completely relaxed. The binding energy between the adsorbent (ad) and the substrate (sub) was defined as E binding =Ead@sub-Esub-Ead, where Ead@sub was the total energy of the substrate with adsorbent intermediates. Esub and Ead are the total energy of substrate and single adsorbent intermediate in vacuum. Gibbs free energy was calculated at 298.15 K in terms of $G=E_{DFT}+ E_{ZPE}$-ts, where E_{DFT} was the electron energy at each step, E_{ZPE} was the zero-point energy, and S was the entropy.

Supplementary Figures and Tables

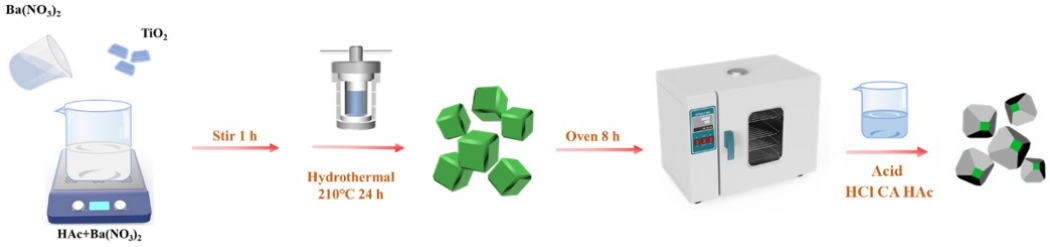

Fig. S1. The synthetic route of the $BaTiO_3$ nanoparticles.

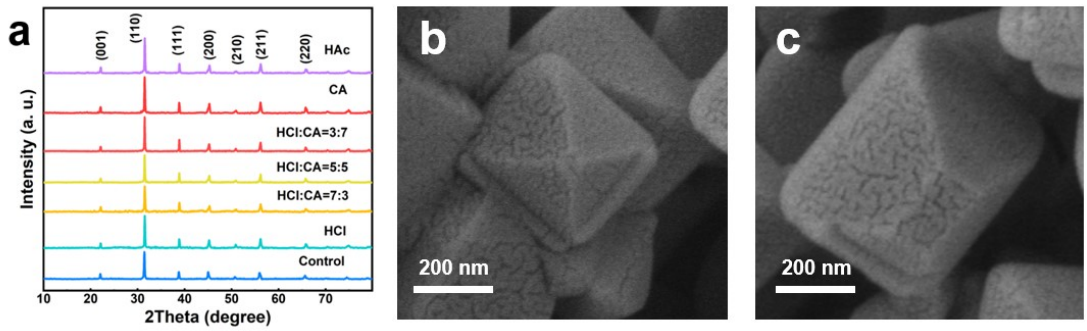

Fig. S2. XRD patterns of $BaTiO_3$ etched by different acids (HCl, HCl:CA=3:7, HCl:CA=5:5, HCl:CA=7:3, CA, HAc).

The diffraction peaks of 22.26°, 31.64°, 38.89°, 45.38°, 51.10°, 56.25°, and 66.12° are corresponded to the crystal planes of (001), (110), (111), (200), (210), (211), and (220), respectively.

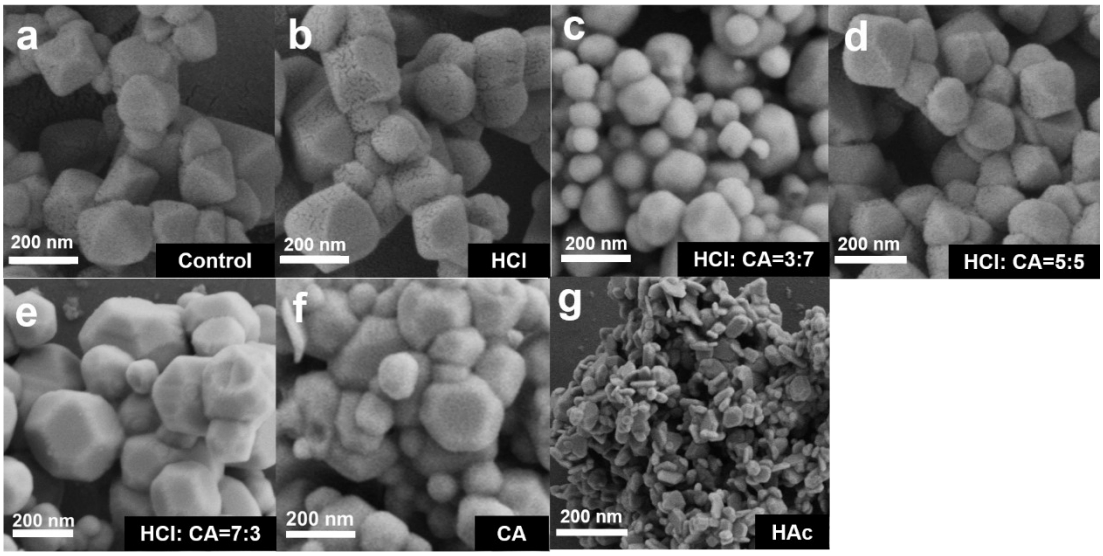

Fig. S3. SEM images: (a) control, (b) HCl, (c) HCl:CA=7:3, (d) HCl:CA=5:5, (e) HCl:CA=3:7, (f) CA, (g) HAc.

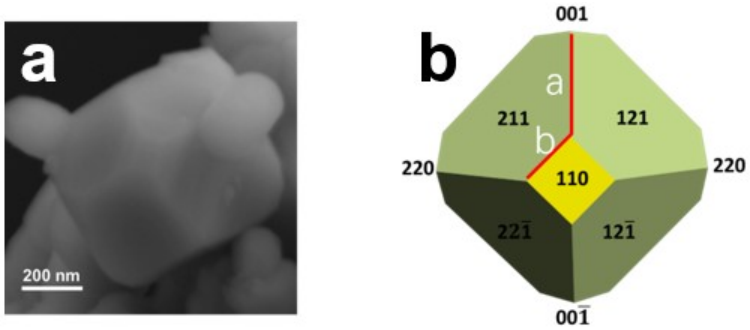

Fig.S4. (a) SEM images of control and (b) Regular octahedral model of tetragonal $BaTiO_3$.

The percentage of the exposed {110} facets in the different samples was calculated using the following equation according to its simulated geometric structure:

$$^{S1}S_{\{110\}\%}=\frac{nb^2}{2(a+\sqrt{3}\ *\ b)^2\sqrt{3}-6b^2\sqrt{3}+6b^2} \qquad \text{(Eq. 1)}$$

Table S1. Exposure ratio of {110} facets of different samples.

Sample	Exposure ratio of {110} facets (%)
control sample	0.00
HCl	1.85
HCl: CA=7:3	7.95
HCl: CA=5:5	30.32
HCl: CA=3:7	55.26
CA	48.63
HAc	41.72

a is the theoretical edge length of regular octahedron, ***b*** is the theoretical side length of (110) facet, ***n*** is the number of {110}.

Table S2. Comparison of photocatalytic product yields in previous work.

Photocatalytic	Light intensity	Products	Yield ($\mu mol \cdot g^{-1} \cdot h^{-1}$)	Ref.
Ag-$BaZrO_3$	300 W Xe lamp	CH_4	0.57	S2
Ag-$H_2SrTa_2O_7$	$\lambda > 200$ nm	CO	0.39	S3
Ag-$BaCeO_3$	300 W Xe lamp	CH_4	0.55	S4
TiO_2	300 W Xe lamp	CH_4	0.48	S5
$SrTiO_3$ $BaTiO_3$	500 W Xe lamp	CH_4	0.28 0.21	S6
Bi_2WO_6/CQDs	> 420 nm	CH_4	0.051	S7
$BaTiO_3/Fe_2O_3$	125 W Hg lamp	CH_4	Selectivity = 22 %	S8
This work	**300 W Xe lamp**	**CO/CH_4**	**0.94/0.9**	**/**

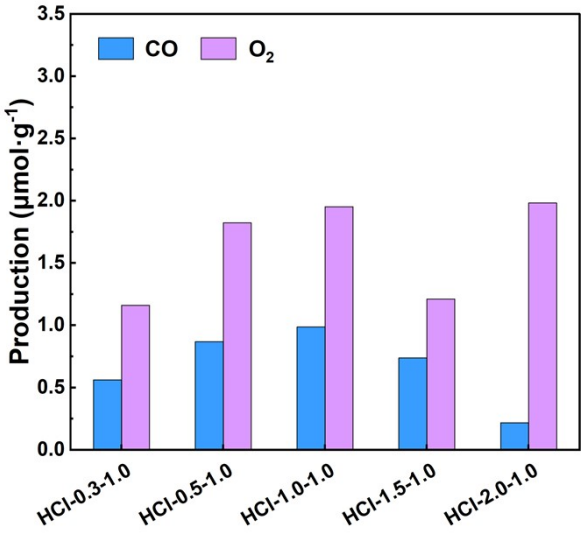

Fig. S5. The evolution rates of $BaTiO_3$ etched by different HCl concentration.

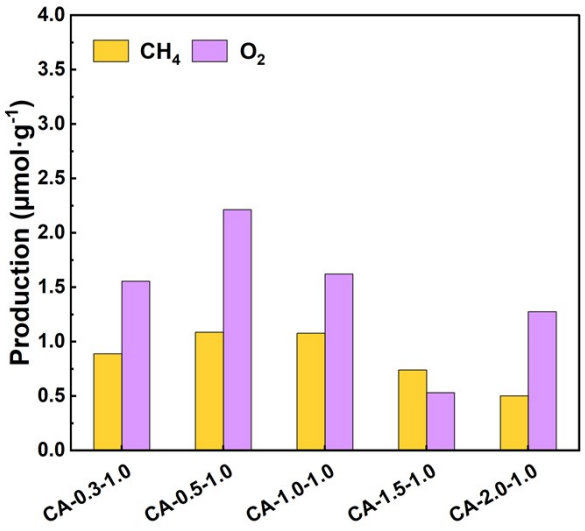

Fig. S6. The evolution rates of $BaTiO_3$ etched by different CA concentration.

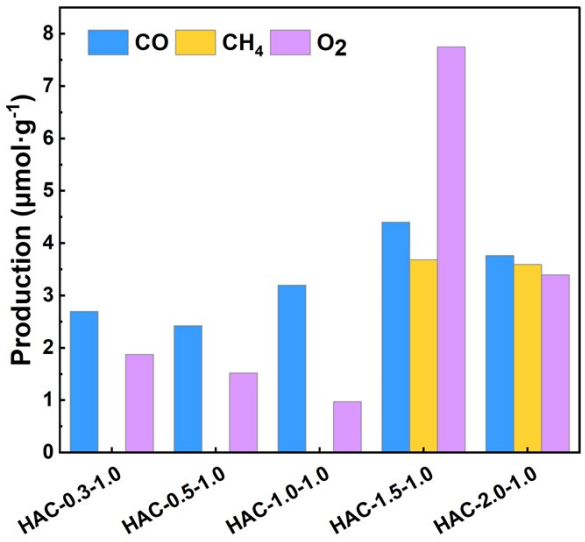

Fig. S7. The evolution rates of $BaTiO_3$ etched by different HAc concentration.

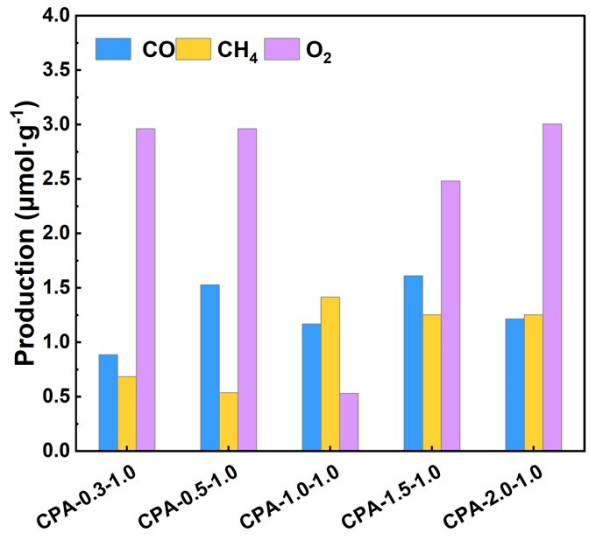

Fig. S8. The evolution rates of $BaTiO_3$ etched by different CPA concentration.

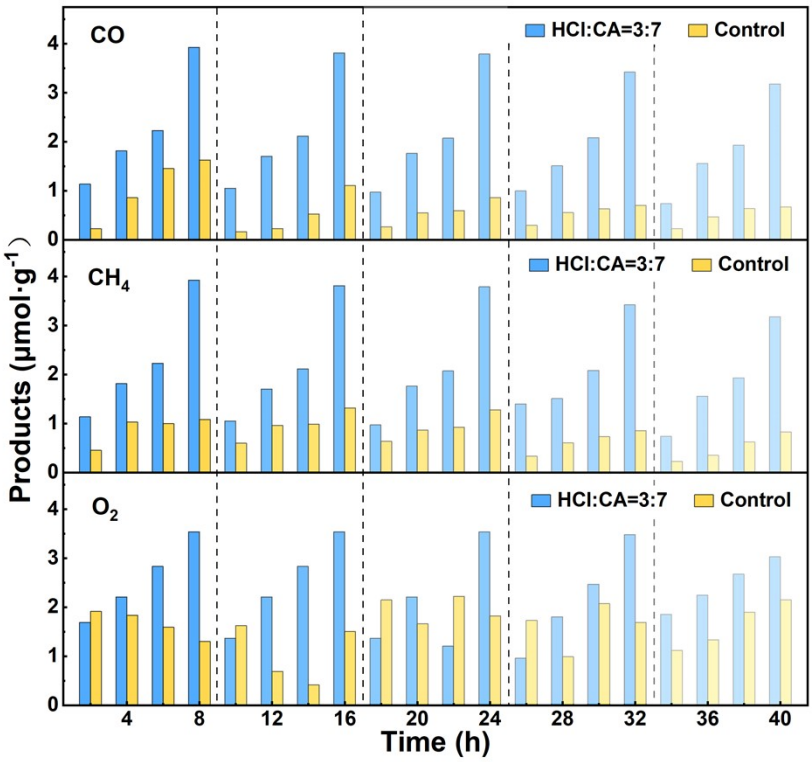

Fig. S9. Cycling runs for the CO_2 reduction of HCl:CA=3:7 and control sample.

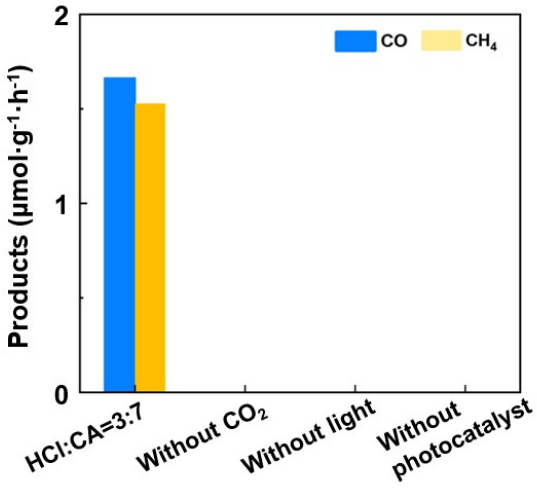

Fig. S10. The CO_2 reduction of HCl:CA=3:7 sample being tested under without CO_2, without light, without photocatalyst conditions.

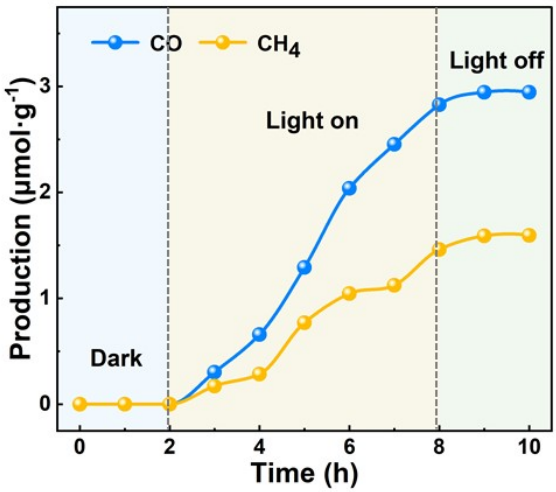

Fig. S11. Yields of CO and CH_4 of HCl:CA=3:7 under dark, light-on, and light-off conditions.

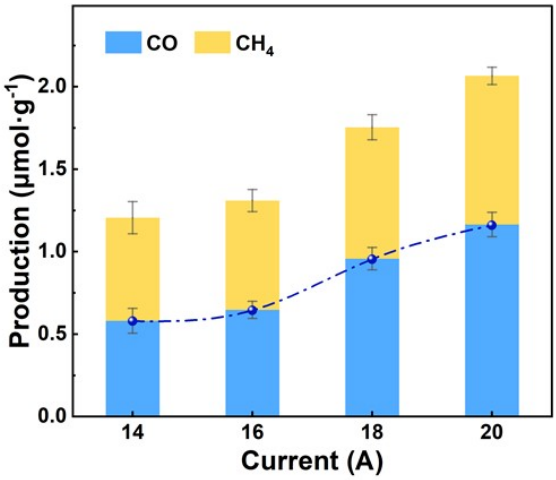

Fig. S12. The product yields of HCl:CA=3:7 under different light intensity.

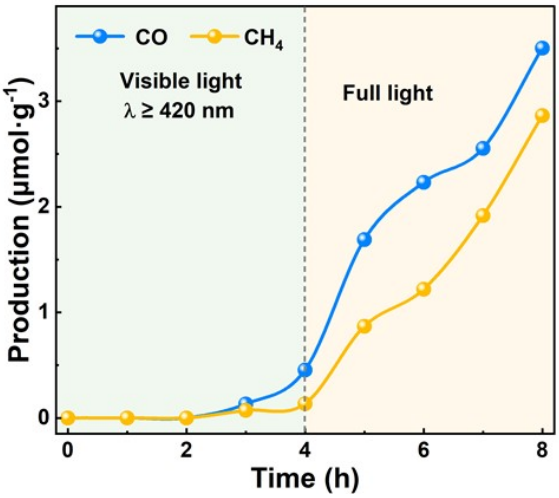

Fig. S13. The CO and CH_4 yield evolutions of HCl:CA=3:7 with 420 nm filter.

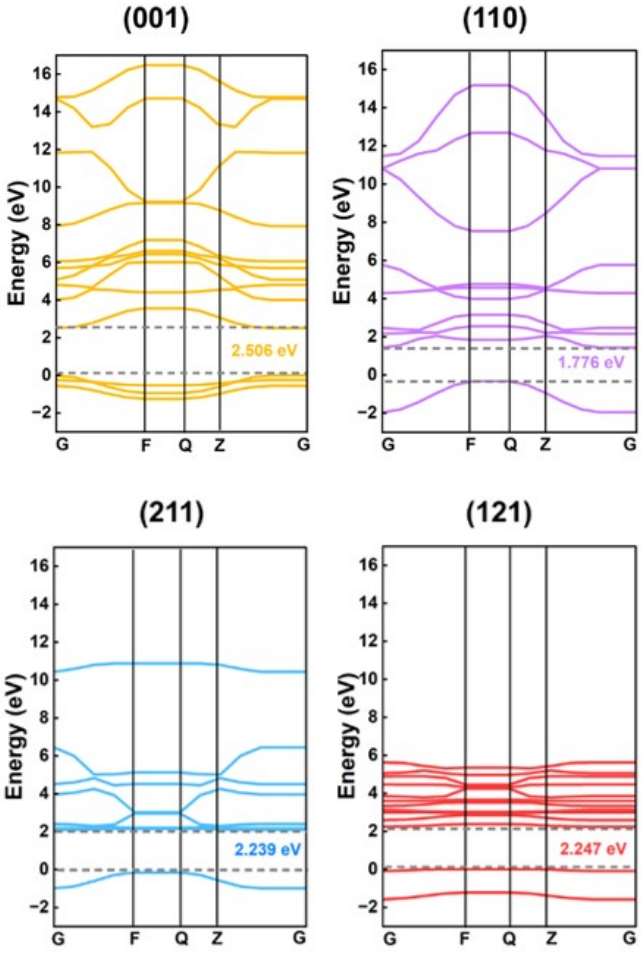

Fig. S14. Electronic band structures of (001), (110), (211), and (121) facets.

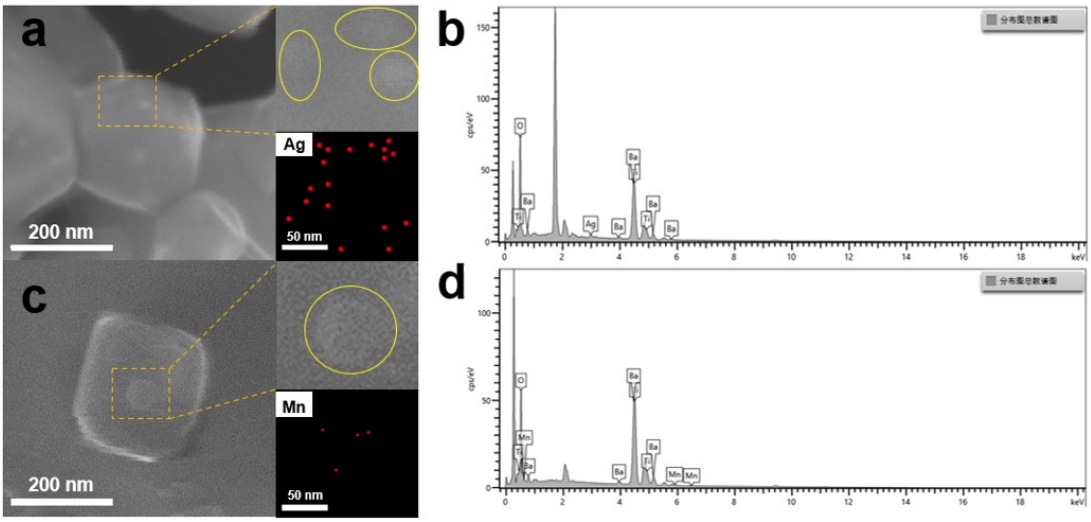

Fig. S15. SEM images and EDX of $BaTiO_3$ photo-deposition with (a,b) Ag and (c,d) MnO_x, respectively.

Table S3. The proportion of Ag and MnO_x deposited on $BaTiO_3$-HCl:CA=3:7.

Element	Wt%	Wt% Sigma	Element	Wt%	Wt% Sigma
O	22.53	0.09	**O**	29.97	0.19
Ti	19.44	0.10	**Ti**	17.78	0.17
Mn	0.60	0.05	**Ag**	1.95	0.10
Ba	57.42	0.13	**Ba**	50.30	0.25
Total	100.00		**Total**	100.00	

Because the side of photogenerated electron is easily susceptible to occur a reduction reaction: $Ag^{+}+e^{-}\rightarrow Ag$, whereas the side of photogenerated hole is more vulnerable to happen an oxidation reaction: $Mn^{2+}+H_2O+(2x\text{-}2)h^{+}\rightarrow MnO_x+2xH^{+}$. Such findings suggest that the structure can facilitate e^{-}-h^{+} pair separation. Meanwhile, the proportion of Ag and MnO_x deposited on HCl:CA=3:7 as shown in Table S3. It is proved the successful deposition of Ag and MnO_x, which is consistent with the previous conclusion. As e^{-} flows from the position with a high contact potential to that with low contact potential.

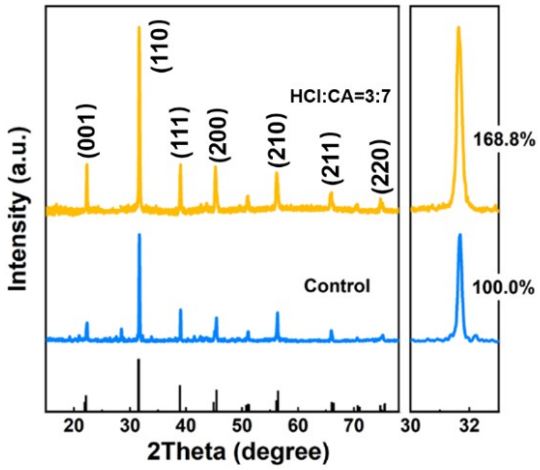

Fig. S16. XRD patterns of control and HCl:CA=3:7 samples after recycling reaction for 40 h.

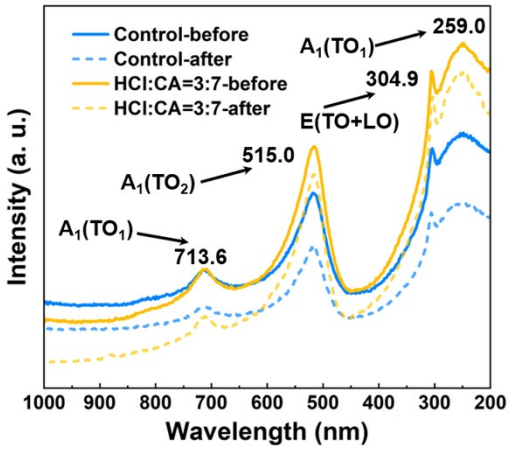

Fig. S17. Raman spectra of control and HCl:CA=3:7 samples after recycling reaction for 40 h.

The Raman peaks at 259.0, 304.9, 515.0 and 713.6 cm^{-1} are the optical phonon modes $A_1(TO)$, $E(TO+LO)$, $A_1(TO_2)$ and $A_1(LO)$ of $BaTiO_3$, respectively[S9]. These peaks are characteristic peaks of the tetragonal phase $BaTiO_3$. The Raman characteristic peaks of control and HCl: CA= 3:7 are not shifted before and after the reaction, which indicates that the crystal phase of the samples can be maintained after the reaction.

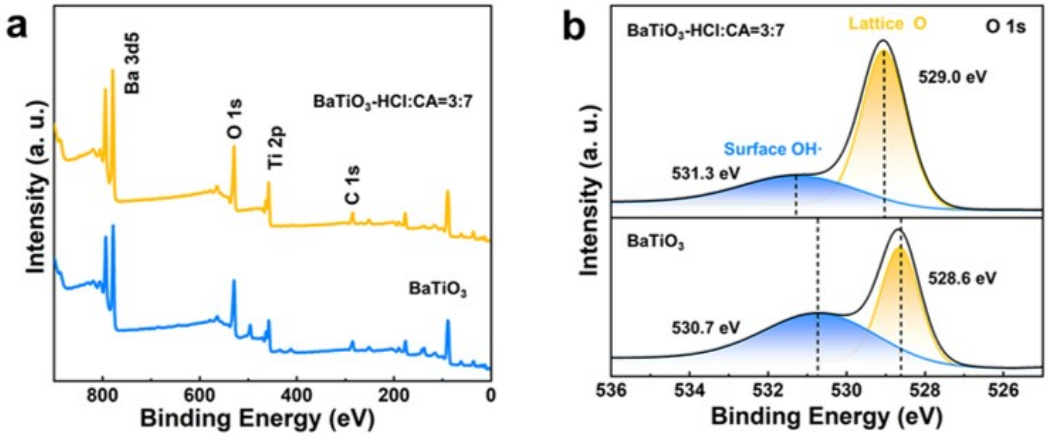

Fig. S18. (a) Survey XPS curves, (b) O 1s of the control sample and HCl:CA=3:7.

Fig. S18a reveals the survey XPS spectra of control sample and HCl:CA=3:7. The high-resolution O 1s spectra in Fig. S18b can be indexed into two distinctive binding energy peaks centered at 528.6 eV and 530.7 eV, which are attributed to the O-Ti and O-Ba (lattice oxygen) and surface OH· on the $BaTiO_3$ surface, respectively[S10].

Table S4. The peak potential of Ba (3d), Ti (2p), and O (1s) by XPS analyses.

Sample	Ba 3d		Ti 2p		O 1s	
	3/2	5/2	1/2	3/2	Surface ·OH	Lattice O
$BaTiO_3$	793.4	778.1	463.2	457.5	530.7	528.6
$BaTiO_3$-HCl:CA=3:7	793.9	778.6	463.6	457.8	531.3	529.0

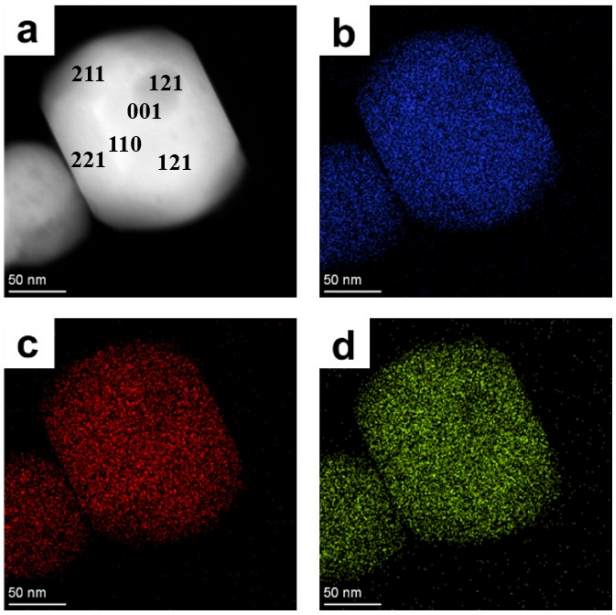

Fig. S19. (a) TEM image. The elemental mapping for $BaTiO_3$-HCl:CA=3:7: (b) Ba, (c) Ti, (d) O.

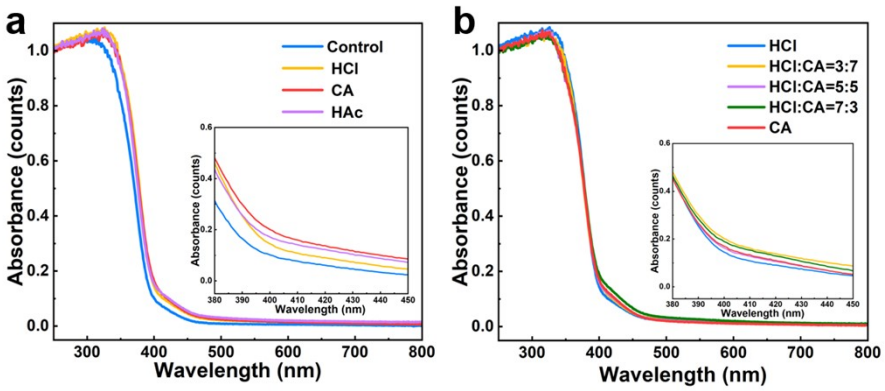

Fig. S20. DRS spectra of (a) $BaTiO_3$-X (control, HCl, CA, HAc) and (b) $BaTiO_3$-X (HCl, HCl:CA=3:7, 5:5, 7:3, CA).

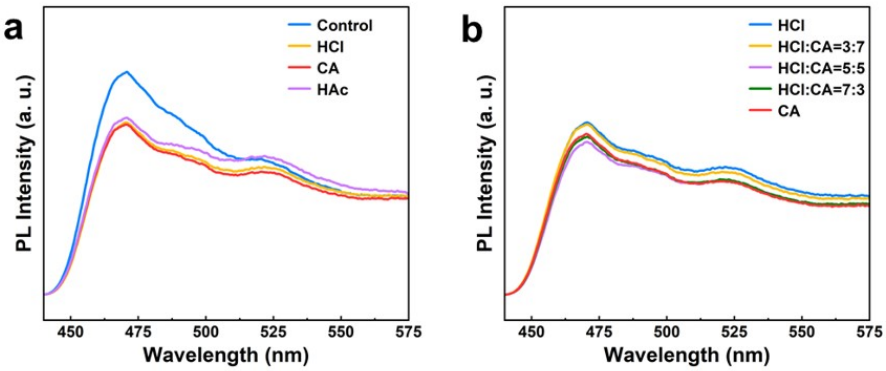

Fig. S21. PL spectra of (a) $BaTiO_3$-X (control, HCl, CA, HAc) and (b) $BaTiO_3$-X (HCl, HCl:CA=3:7, 5:5, 7:3, CA).

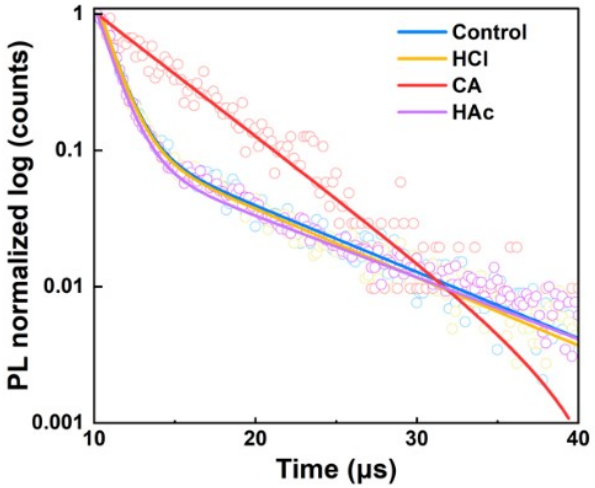

Fig. S22. TRPL spectra of (a) $BaTiO_3$-X (control, HCl, CA, HAc).

Analysis of TRPL decay curves of $BaTiO_3$-X (HCl, CA, HAc, CPA, HCl:CA=3:7, 5:5, 7:3) are fitted with multiple exponential fitting and shown below:

$$^{S11}I(t)=\Sigma_k I_k \exp(-t/\tau_k) \quad \text{(Eq. 2)}$$

where $I(t)$ is the observed ensemble intensity at the time point of t, and I_k and τ_k are the intensity and lifetime of an arbitrary excited state of k, respectively. The PL intensity decays can be well-fitted with bi-exponential decay curves (k=2). The fitting results are summarized in Table S5.

Table S5. Summary of TRPL delay lifetime (τ) and the relative amplitude (*A, %*) for $BaTiO_3$-X (HCl, CA, HAc, CPA, HCl:CA=3:7, 5:5, 7:3), which are fitted by the multiple exponential decays.

Parameters	**A1 (%)**	**τ_1 (μs)**	**A1 (%)**	**τ_2 (μs)**
control	3192.15	1.26	0.2276	10.96
$\tau_{average}$ (μs)		1.26		
HCl	1960.92	1.08	0.1952	8.55
$\tau_{average}$ (μs)		1.09		
CA	9429.55	0.38	4.9637	5.86
$\tau_{average}$ (μs)		0.42		
HAc	2295.12	1.28	0.1335	17.76
$\tau_{average}$ (μs)		1.29		
CPA	3596.93	1.25	0.2090	11.20
$\tau_{average}$ (μs)		1.26		
HCl:CA=3:7	2054.92	1.33	0.1808	12.06
$\tau_{average}$ (μs)		1.34		
HCl:CA=5:5	3813.90	1.24	0.1733	13.29
$\tau_{average}$ (μs)		1.24		
HCl:CA=7:3	2334.21	1.32	0.2068	11.98
$\tau_{average}$ (μs)		1.33		

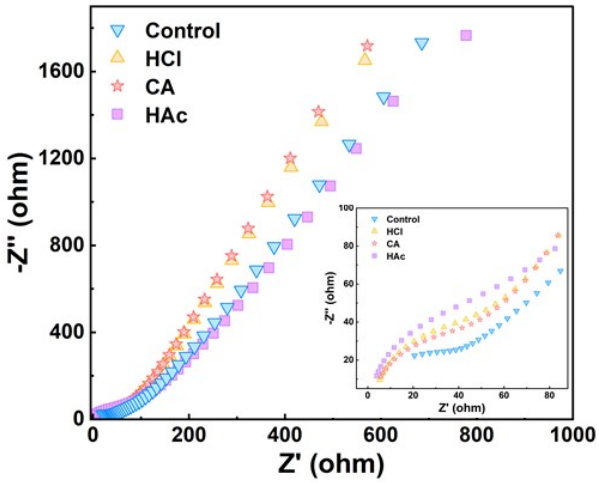

Fig. S23. EIS plots of (a) $BaTiO_3$-X (control, HCl, CA, HAc).

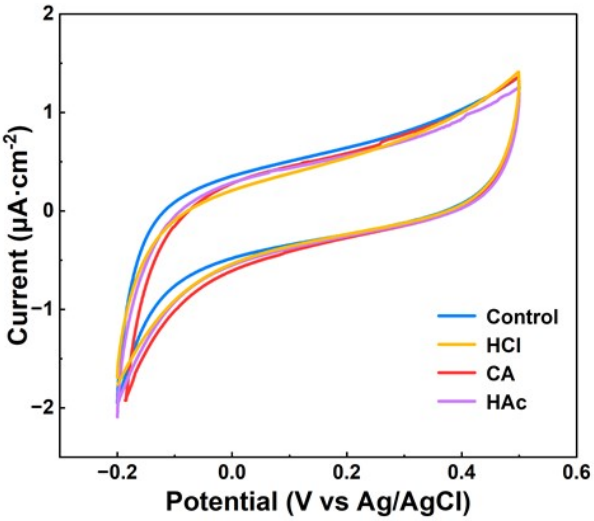

Fig. S24. C-V curves of (a) $BaTiO_3$-X (control, HCl, CA, HAc).

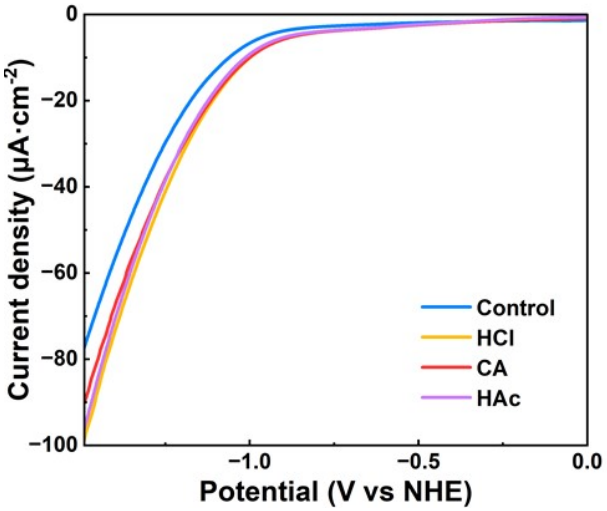

Fig. S25. LSV of (a) $BaTiO_3$-X (control, HCl, CA, HAc).

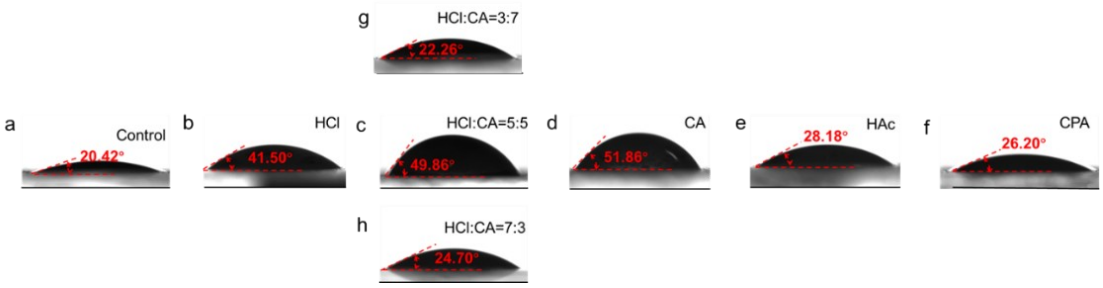

Fig. S26. The static water contact-angle measurements of (a) control sample, (b) HCl, (c) HCl:CA=5:5, (d) CA, (e) HAc, (f) CPA (g) HCl:CA=3:7, (h) HCl:CA=7:3.

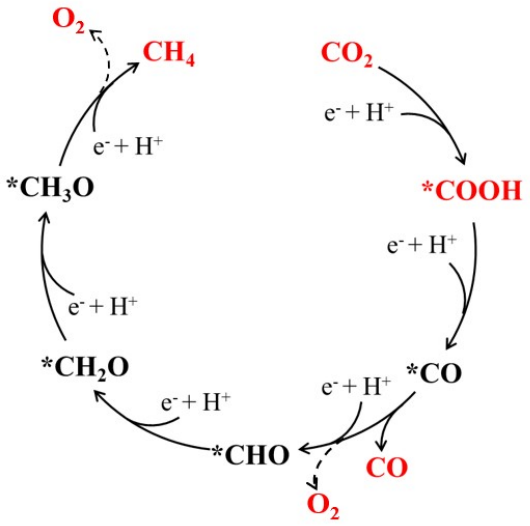

Fig. S27. The reaction process of CO_2 reduction for $BaTiO_3$.

Notes and references

S1 X. Cheng, X. Dao, S. Wang, J. Zhao and W. Sun, *ACS Catal.*, 2020, **11**, 650-658.

S2 X. Chen, J. Wang, C. Huang, S. Zhang, H. Zhang, Z. Li and Z. Zou, *Catal. Sci. Technol.*, 2015, **5**, 1758-1763.

S3 Y. Wang, M. Liu, W. Chen, L. Mao and W. Shangguan, *J. Alloys Compd.*, 2019, **786**, 149-154.

S4 J. Wang, C. Huang, X. Chen, H. Zhang, Z. Li and Z. Zou, *Appl. Surf. Sci.*, 2015, **358**, 463-467.

S5 J. Yu, J. Low, W. Xiao, P. Zhou and M. Jaroniec, *J. Am. Chem. Soc.*, 2014, **136**, 8839-8842.

S6 G. Yang, J. Xiong, M. Lu, W. Wang, W. Li, Z. Wen, S. Li, W. Li, R. Chen and G. Cheng, *J. Colloid Interface Sci.*, 2022, **624**, 348-361.

S7 X. Kong, W. Tan, B. Ng, S. Chai and A. Mohamed, *Nano Res.*, 2017, **10**, 1720-1731.

S8 N. Zangeneh, S. Sharifnia and E. Karamian, *Environ. Sci. Pollut. Res.*, 2020, **27**, 5912-5921.

S9 D. On, L. Vuong, T. Chuong, D. Quang, H. Tuyen and V. Tung, *J Adv Dielectr.*, 2021, **11**, 2150014.

S10 T. Chen, J. Meng, S. Wu, J. Pei, Q. Lin, X. Wei, J. Li and Z. Zhang, *J. Alloys Compd.*, 2018, **754**, 184-189.

S11 L. Mi, Q. Zhang, H. Wang, Z. Wu, Y. Guo, Y. Li, X. Xiong, K. Liu, W. Fu, Y. Ma, B. Wang and X. Qi, *Ceram. Int.*, 2020, **46**, 10619-10633.